*Published online 17 December 2007*

*Nucleic Acids Research, 2008, Vol. 36, No. 3* ***885–896***
*doi:10.1093/nar/gkm1109*

# Probing dynamics of HIV-1 nucleocapsid protein/target hexanucleotide complexes by 2-aminopurine

**S. V. Avilov[1,2], E. Piemont[1], V. Shvadchak[1], H. de Rocquigny[1] and Y. Mély[1,*]**

[1]Institut Gilbert-Laustriat, UMR 7175 CNRS/Université Louis Pasteur (Strasbourg I), Dépt. Pharmacologie et Physicochimie, Faculté de Pharmacie, 74 route du Rhin, 67401 Illkirch, France and [2]Palladin Institute of Biochemistry, 9, Leontovich str., 01030 Kiev, Ukraine

Received August 24, 2007; Revised November 23, 2007; Accepted November 28, 2007

## ABSTRACT

**The nucleocapsid protein (NC) plays an important role in HIV-1, mainly through interactions with the genomic RNA and its DNA copies. Though the structures of several complexes of NC with oligonucleotides (ODNs) are known, detailed information on the ODN dynamics in the complexes is missing. To address this, we investigated the steady state and time-resolved fluorescence properties of 2-aminopurine (2Ap), a fluorescent adenine analog introduced at positions 2 and 5 of AACGCC and AATGCC sequences. In the absence of NC, 2Ap fluorescence was strongly quenched in the flexible ODNs, mainly through picosecond to nanosecond dynamic quenching by its neighboring bases. NC strongly restricted the ODN flexibility and 2Ap local mobility, impeding the collisions of 2Ap with its neighbors and thus, reducing its dynamic quenching. Phe$^{16}$→Ala and Trp$^{37}$→Leu mutations largely decreased the ability of NC to affect the local dynamics of 2Ap at positions 2 and 5, respectively, while a fingerless NC was totally ineffective. The restriction of 2Ap local mobility was thus associated with the NC hydrophobic platform at the top of the folded fingers. Since this platform supports the NC chaperone properties, the restriction of the local mobility of the bases is likely a mechanistic component of these properties.**

## INTRODUCTION

Nucleocapsid protein (NC), either as a domain of the Gag polyprotein precursor or as the mature protein, is essential for several important steps of the virus life cycle (1). For instance, selection of viral genomic RNA for packaging into virions is mediated by NC binding to the ψ encapsidation sequence within the untranslated region of the HIV-1 genome (2). Furthermore, NC chaperones the annealing of the primer tRNA to the primer binding site (PBS), and the two obligatory strand transfers necessary for the synthesis of a complete proviral DNA by reverse transcriptase (3,4). Mature NC is a basic protein of 55 amino acids (Figure 1) containing two highly conserved $CX_2CX_4HX_4C$ zinc fingers (5). Mutations of the zinc coordinating residues and the two aromatic residues of the zinc fingers lead to completely noninfectious viruses (6–9).

Most NC functions rely on interactions with nucleic acid targets. The structure of NC complexed to the SL2 and SL3 stem-loops as well as to the ACGCC sequence of the ψ encapsidation sequence have been solved by NMR (10–12). In all these complexes, the hydrophobic platform formed by the Val$^{13}$, Phe$^{16}$, Thr$^{24}$, Ala$^{25}$, Trp$^{37}$ and Met$^{46}$ residues at the surface of the two folded zinc fingers has been shown to be critical for binding. A particularly important role was notably demonstrated for Trp$^{37}$ that stacks with G residues in all these complexes.

Though 3D structures of NC complexes with several oligonucleotides (ODNs) are available, the dynamics of the ODNs in the complexes is still not well characterized. Dynamics of either single- and double-stranded nucleic acids plays an important role in their interaction with various ligands (13,14). For instance, in the HIV-1 RNA TAR stem-loop, the magnitude of the adaptive structure change due to ligand binding at a given site correlates with the degree of spontaneous internal motions at this site (15). It is likely that the local dynamics of ODNs are important for NC binding and activities as well.

Site-specific information on ODN dynamics can be provided by environmentally sensitive fluorescent probes, such as 2-aminopurine (2Ap), a fluorescent analog of adenine that can be selectively excited at 315–320 nm, where Trp does not absorb (16). The quantum yield of free 2Ap at pH 7.0 is 0.68 (17) but within ODNs it is significantly quenched due to interactions with its neighbor bases (18–22). Free 2Ap in water exhibits a single lifetime

*To whom correspondence should be addressed. Tel: +33 3 90 24 42 63; Fax: +33 3 90 24 43 13; Email: mely@pharma.u-strasbg.fr

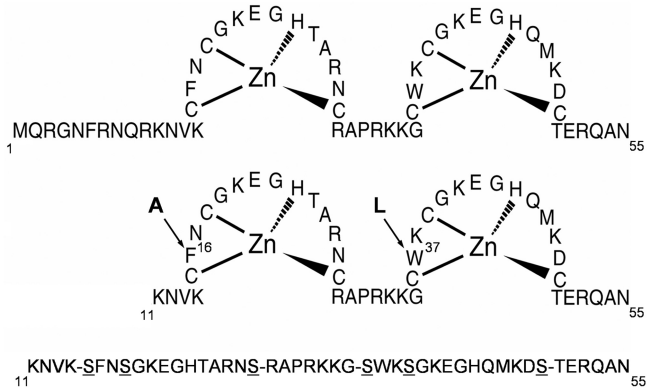


**Figure 1.** Structures of the native and mutated HIV-1 NC peptides used in this study: NC(1-55), NC(11-55), $A^{16}$NC(11-55), $L^{37}$NC(11-55) and $(SSHS)_2$NC(11-55).

of about 10–11 ns, while multiple shorter lifetimes appear when 2Ap is incorporated into ODNs, indicating a highly heterogeneous environment of the probe. As a consequence, time-resolved fluorescence of 2Ap has been largely used to site-specifically characterize the interactions of ODNs with various ligands, including complementary nucleic acids strands and proteins (23–27).

To site-specifically investigate the changes in the dynamics of ACGCC during NC binding and correlate them with the known 3D structure of the NC/ACGCC complex (11), 2Ap was introduced either downstream or upstream to the CG motif. Moreover, since the environment of 2Ap at the 3′ or 5′ terminus of an ODN differs significantly from that at an internal position (18,28), complicating the data interpretation, an extra adenine was added at the 5′-terminus of ACGCC. This extra adenine was shown to not affect the binding of the ODN to NC (29). Moreover, substitutions of A2 and C5 with 2Ap within $^1$AACGCC$^6$ were also expected to not affect NC binding, since the corresponding residues of ACGCC only marginally interact with NC (11). Furthermore, since NC binds with strong affinity to TG motifs (29,30), we studied the interaction of NC with 2Ap-labeled AATGCC sequences. Finally, the native NC was substituted with several NC mutants (Figure 1) to investigate the role of the N-terminal basic domain and the folded finger domain as well as the hydrophobic platform on the top of the fingers on the dynamics of the labeled ODNs.

## MATERIALS AND METHODS

### Materials

NC(1-55) (further referred as NC), NC(11-55), $(SSHS)_2$NC(11-55), $L^{37}$NC(11-55) and $A^{16}$NC(11-55) (Figure 1) were synthesized on a Applied Biosystems A433 peptide synthesizer as described (31). 2Ap-substituted DNA ODNs were synthesized and HPLC-purified by IBA GmbH (Germany). Absorbance spectra were recorded with a Cary 400 UV-visible spectrophotometer (Varian). ODN concentrations were calculated using the extinction coefficients ($\varepsilon_{260}$, $M^{-1} \times cm^{-1}$) of 58 050, 44 190, 51 390, 59 220, 45 360 and 52 560 for AACGCC, AApCGCC, AACGApC, AATGCC, AApTGCC and AATGApC, respectively. All experiments were performed in 50 mM HEPES, pH 7.5, at 20°C. 'Fluorescence microscopy' grade glycerol (Merck, Germany) was used. All other chemicals were purchased from Sigma, USA.

### Steady-state fluorescence spectroscopy

Fluorescence spectra were recorded on FluoroMax3 and FluoroLog spectrofluorimeters (Jobin Yvon) equipped with thermostated cell compartments. Spectra were corrected for screening effects and buffer fluorescence. Quantum yield was calculated using free 2Ap as a reference [0.68 (17)]. 2Ap was excited at 315 nm. To determine the affinity of NC for the 2Ap-labeled ODNs, fixed amounts of NC were titrated with ODNs by monitoring the intrinsic Trp fluorescence of NC at 320-nm emission wavelength (to exclude 2Ap fluorescence). Affinity constants were determined from direct fitting of the experimental signal to the rewritten Scatchard equation:

$$I = I_0 - \frac{(I_0 - I_t)}{P_t} x \frac{\left[ \begin{array}{c} (1 + (P_t + nN_t)K_{app}) \\ -\sqrt{(1 + (P_t + nN_t)K_{app})^2 - 4P_t nN_t K_{app}^2} \end{array} \right]}{2K_{app}} \quad \mathbf{1}$$

where $I$ and $I_t$ are the intensities at a given and a saturating ODN concentration, respectively, $I_0$ is the intensity in the absence of ODN, $N_t$ is the total ODN concentration, $P_t$ is the total concentration of peptide, $K_{app}$ is the apparent affinity constant, $n$ is the number of binding sites. Alternatively, the $K_{app}$ values were also obtained by titrating fixed amounts of 2Ap-labeled ODNs with the peptides and monitoring the 2Ap fluorescence at 370 nm. The data were fitted with a slightly modified version of Equation (1). The parameters were recovered from nonlinear fits of Equation (1) to experimental datasets by the Microcal Origin$^{TM}$ 6.0 program.

### Time-resolved fluorescence measurements

Time-resolved fluorescence measurements were performed with the time-correlated, single-photon counting technique using the excitation pulses at 315 nm provided by a pulse-picked frequency tripled Ti-sapphire laser (Tsunami, Spectra Physics) pumped by a Millenia X laser (Spectra Physics) (32). The emission was collected through a polarizer set at magic angle and an 8-nm band-pass monochromator (Jobin-Yvon H10) at 370 nm. The instrumental response function was recorded with a polished aluminum reflector, and its full width at half-maximum was 40 ps. The mean lifetime $<\tau>$ was calculated from the individual fluorescence lifetimes, $\tau_i$, and their relative amplitudes, $\alpha_i$, according to $<\tau> = \Sigma\alpha_i\tau_i$. The population, $\alpha_0$, of dark species of 2Ap within the ODNs was calculated by: $\alpha_0 = 1 - \tau_{free}/(\tau_{sample} \times R_m)$, where $\tau_{free}$ is the lifetime of free 2Ap, $\tau_{sample}$ is the measured lifetime of 2Ap within the ODN (either free or bound to NC) and $R_m$ is the ratio of the corresponding

steady-state fluorescence intensities. The remaining amplitudes, $\alpha_{ic}$, were recalculated from the measured amplitudes, $\alpha_i$, according to: $\alpha_{ic} = \alpha_i \times (1 - \alpha_0)$.

For time-resolved anisotropy measurements, the fluorescence decay curves were recorded at vertical and horizontal positions of the polarizer and analyzed by the following equations:

$$I_{\parallel}(t) = \frac{I(t)[1 + 2r(t)]}{3}$$

$$I_{\perp}(t) = \frac{I(t)[1 - r(t)]}{3}$$

$$r(t) = \frac{I_{\parallel}(t) - GI_{\perp}(t)}{I_{\parallel}(t) + 2GI_{\perp}(t)} = r_0 \sum \beta_i \exp\left(\frac{-t}{\varphi_i}\right) \quad \mathbf{2}$$

where $\beta_i$ are the amplitudes of the rotational correlation times $\varphi_i$; $I_{||}$ and $I_{\perp}$ are the intensities collected at emission polarizations parallel and perpendicular, respectively, to the polarization axis of the excitation beam, and $G$ is the geometry factor at the emission wavelength, determined in independent experiments. The initial anisotropy value (0.33) was determined independently for 2Ap in 77% glycerol (v/v) from the extrapolation of the anisotropy decay curves to zero time. The theoretical values of the rotational correlation times were calculated from the molecular masses ($M$) of the molecules and their complexes, assuming spherical shapes, by:

$$\varphi = \frac{\eta M(\upsilon + h)}{RT} \quad \mathbf{3}$$

where η is the viscosity (assumed to be 0.01 $P$), $T$ is the temperature (maintained at 293 K), $\nu$ is the specific volume of the particle [assumed to be 0.83 ml/g, (33)], $h$ is the hydration degree (assumed to be 0.2 ml/g for proteins) and $R$ is the molar gas constant.

The cone semiangle ($\theta_0$) providing an estimate for the local motions of 2Ap modeled as diffusion within a cone (34,35) was calculated as:

$$\theta_0 = \cos^{-1}(0.5 \times (\sqrt{1 + 8S} - 1)) \quad \mathbf{4}$$

where $S$ is the generalized order parameter: $S = (\beta'_2/(\beta'_1 + \beta'_2))^{1/2}$, $\beta'_1$ and $\beta'_2$ are the amplitudes of the rotational correlation times, recalculated such that $\Sigma\, \beta'_i = r_0$.

Time-resolved intensity and anisotropy data were treated with a nonlinear least-square analysis (39) using a homemade software (kindly provided by G. Krishnamoorthy). In all cases, the $\chi^2$ values were close to 1, and the weighted residuals as well as the autocorrelation of the residuals were distributed randomly around zero, indicating an optimal fit.

## RESULTS

### 2Ap fluorescence within free hexanucleotides

Fluorescence spectra of the AACGCC and AATGCC sequences labeled by 2Ap at position 2 or 5 showed a maximum emission wavelength at around 370 nm, similarly to free 2Ap (Figure 2). In contrast, the quantum yield

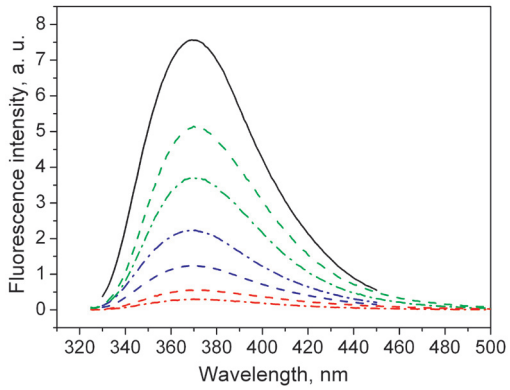


**Figure 2.** Effect of NC and glycerol on the fluorescence spectra of AApCGCC and AACGApC. The fluorescence spectra of AApCGCC (dashed lines) and AACGApC (dash-dotted lines) sequences were recorded in the absence of NC either in buffer (red), in 77% glycerol (green) or in the presence of a 7.5-fold molar excess of NC (blue). Solid line is free 2Ap. Excitation at 315 nm, excitation and emission slits: 2 and 5 nm, respectively.

of 2Ap within ODNs is much lower than that of the free fluorophore (Figure 2), in agreement with the literature (36). The quenching in respect with free 2Ap is more pronounced for 2Ap in the position 5 (38-fold intensity decrease) than in the position 2 (about 19-fold decrease) (Table 1), probably due to the flanking G4 residue, since guanine is the best quencher of 2Ap fluorescence among the bases (37). Moreover, the identical quantum yield of AApCGCC and AApTGCC suggests that 2Ap fluorescence does not depend on the nature of the pyrimidine base in position 3.

Since steady-state fluorescence is unable to report on the dynamics and heterogeneity of the fluorophore microenvironment, time-resolved fluorescence measurements were performed. Four components ranging from ≈100 ps to 5 ns were required for good fitting ($\chi^2 < 1.4$) of the intensity decay curves (Table 1), demonstrating a large conformational heterogeneity of 2Ap in the studied ODNs. Multiple lifetimes are frequently observed in 2Ap-labeled ODNs and are usually associated with partially stacked structures with the shortest component reflecting decay from stacked conformations and the 8–10 ns components assigned to conformations where the 2Ap is extrahelical (37,38). In the studied ODNs, the longest lifetime (4–5 ns) was substantially lower than the lifetime of free 2Ap in water but comparable to that of 2Ap-labeled trinucleotides (19) and single-stranded ODNs (28). By analogy to the latter sequences, nanosecond conformational fluctuations of the 2Ap-labeled hexanucleotides in their excited state can drive 2Ap from an unstacked to a stacked conformation, leading to a fluorescence quenching and thus, a lifetime shortening.

The mean lifetime of 2Ap in the four ODNs (0.91–1.33 ns) was found to be 7.7- to 11.2-fold shorter than that of the free probe (10.2 ns) (Table 1). However, this difference in lifetimes was far less than the 19- to 38-fold difference in the corresponding quantum yields, suggesting the presence of a significant subpopulation of 'dark' species ($\alpha_0$), i.e. species with a lifetime shorter than

**Table 1.** Steady-state and time-resolved fluorescence parameters for 2Ap-substituted hexanucleotides[a]

| | Quantum yield | $R_m$ ($I_{free2Ap}/I$) | $\alpha_0$ | $\tau_1$ (ns) | $\alpha_1$ | $\tau_2$ (ns) | $\alpha_2$ | $\tau_3$ (ns) | $\alpha_3$ | $\tau_4$ (ns) | $\alpha_4$ | $<\tau>$ (ns) |
|---|---|---|---|---|---|---|---|---|---|---|---|---|
| Free 2Ap | 0.680[b] | | | | | | | | | 10.2 | 1.00 | 10.2 |
| AApCGCC | 0.036 | 19.0 | 0.41 | 0.19 | 0.20 | 0.60 | 0.27 | 1.94 | 0.08 | 4.99 | 0.04 | 0.91 |
| AApCGCC, glycerol 77% | 0.289 | 2.35 | 0.11 | 0.39 | 0.21 | | | 3.78 | 0.30 | 8.17 | 0.38 | 4.86 |
| AApCGCC + NC | 0.090 | 7.57 | 0.36 | 0.17 | 0.15 | 0.69 | 0.24 | 2.01 | 0.11 | 6.58 | 0.14 | 2.09 |
| AApCGCC + NC(11-55) | 0.070 | 9.74 | 0.33 | 0.14 | 0.17 | 0.81 | 0.33 | 3.05 | 0.11 | 6.91 | 0.06 | 1.57 |
| AApCGCC + $(SSHS)_2$NC(11-55) | 0.039 | 17.6 | 0.41 | 0.14 | 0.22 | 0.64 | 0.24 | 2.28 | 0.09 | 5.62 | 0.04 | 0.99 |
| AApCGCC + $A^{16}$NC(11-55) | 0.047 | 14.6 | 0.33 | 0.11 | 0.29 | 0.59 | 0.23 | 2.28 | 0.10 | 6.55 | 0.05 | 1.05 |
| AACGApC | 0.018 | 37.4 | 0.79 | 0.08 | 0.10 | 0.55 | 0.04 | 2.20 | 0.04 | 4.93 | 0.03 | 1.27 |
| AACGApC, glycerol 77% | 0.176 | 3.86 | 0.38 | 0.24 | 0.24 | | | 2.60 | 0.10 | 8.18 | 0.28 | 4.25 |
| AACGApC + NC | 0.134 | 5.06 | 0.21 | 0.12 | 0.19 | 0.75 | 0.19 | 3.77 | 0.32 | 7.85 | 0.09 | 2.56 |
| AACGApC + NC(11-55)) | 0.105 | 6.49 | 0.33 | 0.10 | 0.19 | 0.91 | 0.18 | 3.52 | 0.18 | 6.36 | 0.12 | 2.35 |
| AACGApC + $(SSHS)_2$NC(11-55) | 0.020 | 34.0 | 0.80 | 0.08 | 0.09 | 0.72 | 0.04 | 2.79 | 0.05 | 6.01 | 0.02 | 1.49 |
| AACGApC + $A^{16}$NC(11-55) | 0.108 | 6.28 | 0.25 | 0.15 | 0.24 | 0.85 | 0.17 | 3.03 | 0.20 | 5.98 | 0.14 | 2.15 |
| AApTGCC | 0.036 | 18.9 | 0.51 | 0.14 | 0.22 | 0.85 | 0.18 | 2.16 | 0.04 | 5.26 | 0.05 | 1.11 |
| AApTGCC, glycerol 77% | 0.287 | 2.37 | 0.0 | 0.12 | 0.27 | | | 2.03 | 0.23 | 7.60 | 0.50 | 4.30 |
| AApTGCC + NC | 0.147 | 4.62 | 0.20 | 0.20 | 0.17 | 1.04 | 0.30 | 3.49 | 0.15 | 7.54 | 0.18 | 2.77 |
| AApTGCC + NC(11-55) | 0.085 | 7.97 | 0.28 | 0.44 | 0.41 | 1.48 | 0.14 | 3.66 | 0.08 | 6.55 | 0.09 | 1.77 |
| AApTGCC + $(SSHS)_2$NC(11-55) | 0.034 | 19.8 | 0.54 | 0.08 | 0.18 | 0.66 | 0.17 | 2.47 | 0.07 | 6.13 | 0.04 | 1.12 |
| AApTGCC + $A^{16}$NC(11-55) | 0.045 | 15.1 | 0.49 | 0.10 | 0.19 | 0.65 | 0.20 | 2.55 | 0.08 | 6.56 | 0.04 | 1.30 |
| AApTGCC + $L^{37}$NC(11-55) | 0.107 | 6.39 | 0.16 | 0.12 | 0.29 | 0.75 | 0.28 | 2.98 | 0.16 | 7.84 | 0.11 | 1.90 |
| AATGApC | 0.018 | 38.4 | 0.80 | 0.10 | 0.10 | 1.10 | 0.03 | 2.28 | 0.03 | 4.75 | 0.04 | 1.33 |
| AATGApC, glycerol 77% | 0.227 | 3.00 | 0.16 | 0.12 | 0.29 | | | 1.55 | 0.15 | 7.83 | 0.40 | 4.06 |
| AATGApC + NC | 0.125 | 5.45 | 0.25 | 0.12 | 0.22 | 1.02 | 0.18 | 3.81 | 0.30 | 6.58 | 0.05 | 2.50 |
| AATGApC + NC(11-55) | 0.126 | 5.39 | 0.22 | 0.19 | 0.28 | 1.25 | 0.13 | 3.95 | 0.28 | 6.58 | 0.09 | 2.43 |
| AATGApC + $(SSHS)_2$NC(11-55) | 0.018 | 37.7 | 0.81 | 0.09 | 0.09 | 0.80 | 0.04 | 2.83 | 0.04 | 5.97 | 0.02 | 1.39 |
| AATGApC + $A^{16}$NC(11-55) | 0.106 | 6.40 | 0.27 | 0.19 | 0.26 | 1.09 | 0.16 | 3.59 | 0.22 | 6.86 | 0.09 | 2.17 |
| AATGApC + $L^{37}$NC(11-55) | 0.073 | 9.28 | 0.43 | 0.09 | 0.24 | 0.72 | 0.10 | 2.70 | 0.12 | 6.28 | 0.11 | 1.95 |

[a]Experiments were performed with 1–8 μM 2Ap-labeled ODN in 50 mM HEPES, pH 7.5. The concentrations of NC derivatives were at least seven times higher. The amplitude values are corrected for the dark species, as described in Materials and Methods section. Standard deviations are lower than 15% for the quantum yield, 20% for lifetimes (except for $\tau_1$, where they are below 45%), 20% for amplitudes and 15% for the mean lifetimes, respectively.
[b]Data from Ref. (17).

the detection limit of our equipment (≈30 ps) (Table 1). Generally, such apparently 'null' lifetime may appear as a result of either static quenching or very fast dynamic quenching. To discriminate between 'true' static and fast dynamic quenching, we studied the effect of viscosity on 2Ap fluorescence since only dynamic quenching is affected by viscosity. We observed that in 77% glycerol (v/v), both the quantum yield and the mean lifetime strongly increased (Table 1). Moreover, the number of components needed for good fitting of the decay curves dropped to 3, suggesting a less heterogeneous 2Ap microenvironment. All the observed lifetimes were substantially longer than in the absence of glycerol. The longest component became close to the lifetime of free 2Ap and its amplitude grew to 28–50%, indicating that a large subpopulation of 2Ap does not interact with its neighbors during the excited state lifetime in this case. Moreover, $\alpha_0$ dramatically decreased at high viscosity (Table 1), demonstrating that the 'null' lifetime mostly represents ultra-fast dynamic quenching. The corresponding ultra-short lifetime that cannot be measured with our device likely corresponds to the 10-ps lifetime measured with a streak camera for 2Ap within single-stranded DNAs (39). Interestingly, $\alpha_0$ values for ODNs labeled at position 5 were much higher than for ODNs labeled at position 2, probably due to the flanking G4 residue which causes a more efficient quenching than other bases (21,24,39).

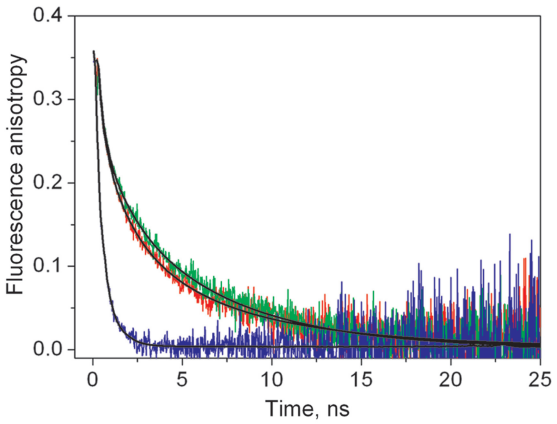


**Figure 3.** Experimental anisotropy decay curves of the 2Ap-labeled ODNs and their complexes. AApCGCC alone (blue), AApCGCC/NC (green) and AACGApC/NC (red). The corresponding fitted curves, using the parameters in Table 2 are in black.

Fluorescence anisotropy decay curves (Figure 3) of the 2Ap-labeled ODNs were fitted adequately with a two-exponential model (Table 2). Since the slower component $\varphi_2$ (0.68–0.83 ns) is slightly shorter than the 1 ns theoretical correlation time for the tumbling of a sphere with the same molecular mass than the ODN (33),

**Table 2.** Fluorescence anisotropy decay parameters for 2Ap-substituted hexanucleotides[a]

| | $\varphi_1$ (ns) | $\beta_1$ | $\varphi_2$ (ns) | $\beta_2$ | $S$ | $\theta_0$ (degree) |
|---|---|---|---|---|---|---|
| 2Ap | 0.08 | 1.00 | | | 0 | 90.0 |
| AApCGCC | 0.28 | 0.59 | 0.83 | 0.41 | 0.633 | 42.9 |
| AApCGCC + NC | 0.30 | 0.38 | 4.31 | 0.62 | 0.787 | 31.8 |
| AApCGCC + NC(11-55) | 0.34 | 0.43 | 3.10 | 0.57 | 0.755 | 34.2 |
| AApCGCC + $(SSHS)_2$NC(11-55) | 0.24 | 0.61 | 2.21 | 0.39 | 0.625 | 43.4 |
| AApCGCC + $A^{16}$NC(11-55) | 0.36 | 0.44 | 3.11 | 0.56 | 0.755 | 34.2 |
| AACGApC | 0.18 | 0.57 | 0.76 | 0.43 | 0.656 | 41.7 |
| AACGApC + NC | 0.46 | 0.42 | 4.08 | 0.58 | 0.762 | 33.9 |
| AACGApC + NC(11-55) | 0.35 | 0.41 | 3.17 | 0.59 | 0.768 | 32.9 |
| AACGApC + $(SSHS)_2$NC(11-55) | 0.30 | 0.61 | 2.21 | 0.39 | 0.625 | 43.8 |
| AACGApC + $A^{16}$NC(11-55) | 0.43 | 0.41 | 3.52 | 0.59 | 0.768 | 33.2 |
| AApTGCC | 0.23 | 0.56 | 0.74 | 0.44 | 0.663 | 40.8 |
| AApTGCC + NC | 0.26 | 0.39 | 4.13 | 0.61 | 0.781 | 32.2 |
| AApTGCC + NC(11-55) | 0.33 | 0.40 | 3.04 | 0.60 | 0.775 | 32.7 |
| AApTGCC + $(SSHS)_2$NC(11-55) | 0.32 | 0.67 | 1.99 | 0.33 | 0.575 | 47.1 |
| AApTGCC + $A^{16}$NC(11-55) | 0.38 | 0.37 | 3.00 | 0.63 | 0.794 | 31.2 |
| AApTGCC + $L^{37}$NC(11-55) | 0.42 | 0.36 | 3.86 | 0.64 | 0.802 | 30.6 |
| AATGApC | 0.14 | 0.54 | 0.68 | 0.46 | 0.678 | 39.7 |
| AATGApC + NC | 0.50 | 0.45 | 4.33 | 0.55 | 0.742 | 34.2 |
| AATGApC + NC(11-55) | 0.52 | 0.41 | 3.45 | 0.59 | 0.768 | 33.2 |
| AATGApC + $(SSHS)_2$NC(11-55) | 0.31 | 0.69 | 2.27 | 0.31 | 0.554 | 48.3 |
| AATGApC + $A^{16}$NC(11-55) | 0.44 | 0.41 | 3.23 | 0.59 | 0.768 | 33.2 |
| AATGApC + $L^{37}$NC(11-55) | 0.28 | 0.44 | 3.03 | 0.56 | 0.751 | 34.0 |

[a]$\beta_1$ and $\beta_2$, the amplitudes of the components; $S$, generalized order parameter; $\theta_0$, cone semi-angle for 2Ap local motion (calculated as described in Materials and Methods section). Standard deviations are <10% for the amplitudes, <30% for $\varphi_1$ and <20% for $\varphi_2$.

the $\varphi_2$ component likely represents a combination of both tumbling and segmental motions, in line with the high flexibility expected for single-stranded ODNs. Moreover, the faster component $\varphi_1$ (0.14–0.28 ns) can be attributed to the local motion of 2Ap in the ODNs (37). The relative amplitude ($\beta_1$) of this faster component allowed to estimate the angular range of the local motion of 2Ap modeled as the diffusion in a cone semi-angle ($\theta_0$) [Equation (4)] (34,37). In further keeping with the high flexibility of the ODNs, rather large $\theta_0$ values were obtained (40–43°) indicating an important rotational freedom for 2Ap (Table 2). Noticeably, since the most quenched conformations (with lifetimes below 0.3 ns) contribute very little (<10%) to the total fluorescence intensity, the calculated diffusion angle likely describes mainly the local motion of the less quenched conformations.

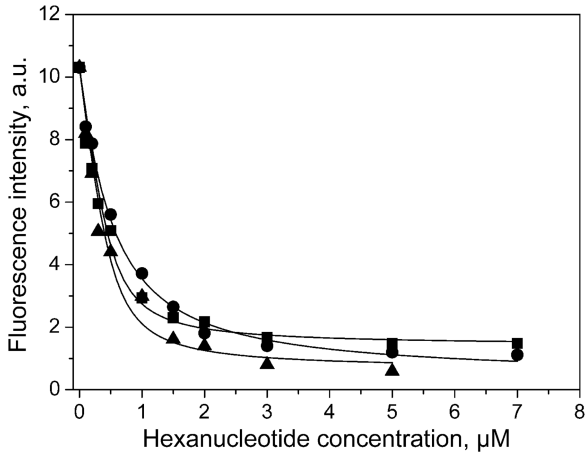


**Figure 4.** Effect of 2Ap substitution on the binding of NC(11-55) to AACGCC. The concentration of NC(11-55) was 1 μM in 50 mM HEPES, pH 7.5. The concentration of AApCGCC (filled circles), AACGApC (filled triangles) and AACGCC (filled squares) is expressed in strands. Solid lines correspond to the fit of the experimental points with Equation (1) and the parameters are given in the text.

## Effects of NC on the dynamics of the 2Ap-labeled hexanucleotides

Our objective was to characterize site-selectively the interaction of NC with the AACGCC and AATGCC sequences, by using 2Ap-labeled ODNs. However, this approach is only valid if the substitution of a natural base by 2Ap does not modify the interaction of NC with the ODNs. To check this, we compared the binding of the 2Ap-labeled sequences with the corresponding unlabeled sequences. The binding parameters were determined by monitoring the Trp emission at 320 nm (where 2Ap does not fluoresce) in the presence of increasing ODN concentrations in 50 mM HEPES, pH 7.5 (Figure 4). Due to the limited sensitivity of Trp fluorescence that does not permit to work at very low protein concentrations, binding experiments were performed with the NC(11-55) peptide that binds in the same way than the native NC, but with a lower affinity (29,40). $K_{app}$ values of $4(\pm1)\times10^6\,M^{-1}$, $9(\pm4)\times10^6\,M^{-1}$ and $9(\pm3)\times10^6\,M^{-1}$ were found for AApCGCC, AACGApC and AACGCC, respectively. For the two last sequences, similar affinities were obtained by monitoring the changes in the 2Ap fluorescence when adding increasing peptide concentrations (data not shown). Accordingly, no change in affinity accompanied the C→2Ap substitution at position 5. This result may be rationalized from the NMR data of the ACGCC/NC

complex showing that NC binds the corresponding C residue only through a single H-bond with its N4 atom (11). It is thus likely that the N7 atom of 2Ap forms the same H-bond with NC since it is located virtually at the same place than the N4 atom in cytosine relatively to the sugar-phosphate axis (11). For AApCGCC, a limited affinity decrease was observed in respect with the native ODN. Since NMR showed no direct interaction between the corresponding A residue with NC, 2Ap may indirectly decrease the binding constant, by decreasing for instance the interaction of the neighbor C residue with NC. Since AATGCC was shown to bind NC much stronger than AACGCC (29), we used a buffer containing 0.1 M NaCl to get reliable binding constants with this ODN. No decrease of NC affinity for AATGApC appeared ($K_{app} = 5(\pm3) \times 10^6\,M^{-1}$) as compared to AATGCC ($K_{app} = 4(\pm1) \times 10^6\,M^{-1}$) whereas the affinity for AAp TGCC ($K_{app} = 8(\pm2) \times 10^6\,M^{-1}$) was slightly higher. As a consequence, 2Ap does not perturb significantly the interaction of the studied ODNs with NC and thus can be reliably used to probe the NC/ODN complexes.

Binding of NC was found to strongly increase the quantum yield of 2Ap within all species, although to different extents: from 2.5-fold for AApCGCC to more than 7-fold for AACGApC (Figure 2 and Table 1). Meanwhile, the position of the emission maximum did not change (Figure 2). Thus, NC binding significantly reduces the quenching of 2Ap fluorescence by its neighbor bases but does not change the polarity of its surrounding. As in the absence of NC, the time-resolved intensity decay of 2Ap within the ODN/NC complexes needed four lifetimes for good fitting. In the complexes, the 2Ap fluorescence decayed slower than in the absence of NC, with an increase in the mean lifetime by a factor of about two (Table 1). Significant differences appear as a function of the labeled position and the ODN nature. For AApCGCC, the increase in the mean lifetime is fully consistent with the quantum yield increase, indicating that NC negligibly affects $\alpha_0$ in this case. In fact, the NC-induced increase in both the quantum yield and mean lifetime of this ODN is essentially due to an increase of the $\alpha_4$ and $\tau_4$ values. Since the $\tau_4$ value approaches the lifetime of free 2Ap, unstacked conformers are probably driven less rapidly than in the free ODN to quenched conformers by conformational fluctuations. For AACGApC and the 2Ap-labeled TG-containing sequences, the NC-induced increase in quantum yield was found to be much higher than the increase in the mean lifetime, suggesting that NC dramatically decreases the $\alpha_0$ value and thus, the ultra-fast dynamic quenching of 2Ap in these ODNs. This decrease in $\alpha_0$ is accompanied by a large increase of the $\alpha_2$ to $\alpha_4$ values as well as an increase of the $\tau_3$ and $\tau_4$ values. Consequently, NC shifts the equilibrium of the 2Ap sub-populations to the less quenched ones and decreases the quenching efficiency in the latter. Interestingly, the effect of NC appears quite homogeneous since NC increases the summed populations ($\alpha_3 + \alpha_4$) of the two less quenched 2Ap conformers from about 10% to 35–40% in all three ODNs.

The effect of NC was found to be quite similar on the time-resolved anisotropy decays of the various 2Ap-labeled ODNs (Figure 3 and Table 2). In all cases, NC induces a striking increase of the $\varphi_2$ component, in line with the formation of NC/ODN complexes. The measured $\varphi_2$ values are significantly higher than the theoretical 3.3 ns value calculated for the tumbling of a 1 : 1 complex with a spherical shape. Thus, the shape of the complexes likely deviates from a sphere and, in contrast to the free ODNs, the $\varphi_2$ component only describes the tumbling motion of the complex, with no contribution of segmental motions. As a consequence, the binding of NC reduces the degrees of freedom of the ODNs. This conclusion is further substantiated by the decrease of the amplitude associated with the local motion. This decrease corresponds to a reduction by 6° to 11° of the cone semi-angle in which 2Ap rotates. Moreover, NC was found to also increase the value of the $\varphi_1$ component for 2Ap at position 5, but not in position 2, indicating that the binding of NC directly altered the flexibility of the 2Ap base at position 5. As in the free ODNs, the conclusions on the local mobility of 2Ap in the complexes probably concern mainly the less quenched subpopulations that contribute strongly to the total fluorescence intensity.

### Effects of NC variants on the local dynamics of the 2Ap-labeled hexanucleotides

To determine the contributions of the N-terminal basic domain, the folded zinc fingers and the conserved aromatic residues ($Phe^{16}$ and $Trp^{37}$) to the effects of NC on the dynamics of the 2Ap-labeled ODNs, we analyzed the fluorescence properties of these ODNs complexed with various NC mutants (Figure 1). The contribution of the N-terminal domain was investigated with the NC(11-55) mutant which includes the zinc finger domain but lacks the N-terminal domain. The contribution of the folded fingers was analyzed with the $(SSHS)_2$NC(11-55) mutant where all cysteines are substituted for serines, which prevents the binding of zinc and therefore the folding of the peptide (8). The contributions of the conserved $Phe^{16}$ residue in the proximal finger and the conserved $Trp^{37}$ residue in the distal finger were investigated by using the $A^{16}$NC(11-55) mutant with $Phe^{16}$ replaced by Ala and $L^{37}$NC(11-55) with $Trp^{37}$ replaced by Leu, respectively. Since both $Phe^{16}$ and $Trp^{37}$ residues do not participate to zinc binding (41), their substitution is expected to not alter the zinc-driven folding of the $A^{16}$NC(11-55) and $L^{37}$NC(11-55) mutants. In contrast, since both residues participate to the hydrophobic plateau at the top of the folded zinc fingers, substantial alterations in this plateau should occur, likely explaining the significant alterations of the binding of the corresponding NC mutants to their ODN targets (7,40,42).

Both the steady-state and time-resolved fluorescence parameters of the complexes of NC(11-55) with AApCGCC, AACGApC and AATGApC were similar to those of the corresponding complexes with the native NC, suggesting that the NC-induced changes in the dynamics of these 2Ap-labeled ODNs are mediated by the zinc finger domain. In contrast to the aforementioned ODNs, an ~2-fold decrease in the quantum yield and the amplitudes associated with the $\tau_3$ and $\tau_4$ lifetimes was

observed when NC was substituted with NC(11-55) in its complex with AApTGCC. Thus, the N-terminal basic domain of NC likely contributes to the NC-induced changes of the local dynamics of 2Ap in this ODN (Table 1). Noticeably, the $\varphi_2$ correlation time of all tested ODNs was substantially lower in their complexes with the truncated mutant than with the native NC. This may be rationalized by the smaller molecular weight of the truncated peptide and probably, the more spherical shape of its complexes with the ODNs (Table 2).

In sharp contrast to NC and NC(11-55), the unfolded $(SSHS)_2$NC(11-55) mutant induced only limited changes in the steady-state and time-resolved parameters of the 2Ap-labeled ODNs. For instance, neither the quantum yield nor the $\alpha_0$, $\alpha_1$ and $\tau_1$ values were significantly affected by $(SSHS)_2$NC(11-55), indicating that the peptide does not affect 2Ap in the most quenched conformers. In contrast, slight increases of about 0.3–0.6 ns and 1 ns were observed for the $\tau_3$ and $\tau_4$ values, respectively, indicating that $(SSHS)_2$NC(11-55) interacts with 2Ap in the less quenched conformers. The limited changes in the time-resolved intensity parameters were not due to poor binding, since this peptide was found to bind even stronger than NC(11-55) to the various target ODNs (data not shown), in line with previous data on other ODNs (43). Moreover, $(SSHS)_2$NC(11-55) increased the $\varphi_2$ correlation time of all 2Ap-labeled ODNs from 0.68–0.83 ns to 2–2.2 ns, confirming that this peptide binds to the ODNs. The correlation time of the complex is substantially lower than the 2.8 ns correlation time expected for the tumbling of a spherical 1:1 complex, indicating that the $\varphi_2$ component describes a combination of tumbling and segmental motions. Thus, $(SSHS)_2$NC(11-55) decreases the overall flexibility of the ODNs to a lesser extent than NC and NC(11-55).

Substitution of the $Phe^{16}$ residue by Ala in the $A^{16}$NC(11-55) mutant was found to decrease the affinity for the various ODNs by about 20-fold (data not shown), in line with a significant contribution of $Phe^{16}$ in the binding process (42). Nevertheless, at the high concentrations needed for the time-resolved experiments, we calculated that more than 80% of the 2Ap labeled ODNs were bound to $A^{16}$NC(11-55). Substitution of NC(11-55) by $A^{16}$NC(11-55) only marginally altered the amplitudes associated with the different fluorescence lifetimes as well as the time-resolved anisotropy parameters of the ODNs labeled by 2Ap at the 5 position (Tables 1 and 2). The only significant change was the decrease of the $\tau_3$ to $\tau_4$ values, suggesting that $A^{16}$NC(11-55) reduces less efficiently than NC(11-55) the quenching of 2Ap fluorescence by its neighbor bases in these conformations. As a consequence, the $Phe^{16}\rightarrow$Ala mutation induces only subtle changes in the interaction of NC with 2Ap at position 5. In sharp contrast, strong differences between NC(11-55) and $A^{16}$NC(11-55) were observed when the two peptides interact with ODNs labeled at position 2. Indeed, the quantum yield and time-resolved intensity values of both AApCGCC and AApTGCC derivatives were much lower in the presence of $A^{16}$NC(11-55) than in the presence of NC(11-55) and approached the values of the free ODNs, indicating that substitution of $Phe^{16}$ with Ala prevented modifications of the local dynamics of 2Ap at position 2. However, the values of the longer correlation time of AApCGCC and AApTGCC bound with $A^{16}$NC(11-55) and NC(11-55) were indistinguishable, indicating that both peptides decrease the overall flexibility of the ODNs to the same extent. Moreover, the two peptides provide similar $\beta_1$ values, suggesting that they similarly restrict the amplitude of the 2Ap motion.

Substitution of $Trp^{37}$ by Leu dramatically decreased (by two orders of magnitude) the binding constants of NC to the various ODNs, in line with the critical role of $Trp^{37}$ in nucleic acid recognition (6,10,11,29,44–48). As a consequence, only the more affine TG-containing ODNs could be used to obtain a sufficient level of binding (> 80%) in the time-resolved experiments. NC(11-55) and $L^{37}$NC(11-55) were found to substantially differ in their ability to alter the time-resolved fluorescence intensity parameters of the AATGApC sequence (Table 1). Indeed, the $L^{37}$NC(11-55) mutant induced about two times lower increase than NC(11-55) in the quantum yield of AATGApC, due to its lower efficiency in shifting the populations of the more quenched species toward the less quenched ones. Nevertheless, the $L^{37}$NC(11-55) mutant significantly increased the $\tau_3$ and $\tau_4$ values of AATGApC as well as their associated amplitudes, indicating that the mutated peptide was able to interact with the less stacked conformers, though less efficiently than the unmodified NC(11-55) peptide. In contrast to AATGApC, only limited differences in the fluorescence parameters of AApTGCC were observed in its complexes with NC(11-55) and $L^{37}$NC(11-55) (Table 1), suggesting that the $Trp^{37}\rightarrow$Leu mutation affects essentially the ability of NC to perturb the local kinetics of 2Ap at position 5. This conclusion was further substantiated by the different effects of $L^{37}$NC(11-55) and NC(11-55) on the value of the short rotational correlation time of 2Ap at position 5, but not at position 2 (Table 2). In contrast to NC(11-55), the $L^{37}$ mutant only moderately slowed down the local motion of 2Ap at position 5.

## DISCUSSION

In this study, we investigated the steady state and time resolved fluorescence properties of 2Ap-substituted AACGCC and AATGCC sequences and their complexes with native and mutated NC proteins. In the absence of NC, the complex intensity decays with four resolved lifetimes and one nonmeasurable 'null' lifetime suggest that 2Ap adopts at least five different conformations in these ODNs (18,49). Probably, even more geometries are explored but cannot be experimentally observed due to the limited resolution of the time-resolved measurements. The very low quantum yield as well as the time-resolved fluorescence parameters (and notably the absence of a free 2Ap-like component) of the 2Ap-labeled hexanucleotides are reminiscent of those previously observed with 2Ap-labeled trinucleotides (19). In further analogy with the latter sequences, a dramatic fluorescence increase of the 2Ap-labeled hexanucleotides was observed in a viscous

medium, due to a strong decrease of the population of the most quenched conformers and a corresponding increase of the population of the less quenched conformers (Table 1). The fluorescence quenching of 2Ap appears thus highly dynamic and results probably from a charge transfer mechanism occurring during its collisions with its neighbors (19,20). This mechanism is in line with the strong quenching observed when 2Ap is next to a guanine, since this last residue shows the lowest redox potential among the bases (21,22,39). These fluorescence properties of the labeled hexanucleotides largely rely on their highly flexible structure, which allows conformational fluctuations in the picosecond–nanosecond (ps–ns) range. The high flexibility of the ODNs is substantiated by the large amplitude associated with their short correlation time as well as by the low value of their long rotational correlation time, showing strong contributions of both local and segmental motions that prevent observation of the tumbling motion. In this respect, even if unstacked 2Ap conformations are excited, rapid conformational changes will bring 2Ap close to one of its neighbor, allowing charge transfer and thus, fluorescence quenching. Moreover, the 'null' lifetime likely corresponds to a conformation where 2Ap stacks with one of its neighbors, leading to an almost immediate quenching.

Binding of NC induces a strong decrease of the ODN flexibility, with notably a disappearance of the segmental motions, as shown by the values of the long rotational correlation times (Table 2). This decrease in ODN flexibility is consistent with the well-resolved structure of ACGCC in its complex with NC(12-53) (11) as well as with the 'freezing' by NC of the nanosecond dynamics of a dsDNA (50). The effect of NC on ODN flexibility is in line with an 'adaptive binding' mechanism where a flexible nucleic acid sequence becomes more ordered upon binding of a protein (51,52). As a consequence of this decreased flexibility, collisions of 2Ap with its neighbors needed for fluorescence quenching are restricted, explaining the increased quantum yields and the shift toward the less quenched populations (associated with the longer lifetimes) in the presence of NC. In addition, NC also affects the local motion of 2Ap at positions 2 and 5 by decreasing its excursion angle, in full line with the NMR structure of the ACGCC/NC(12-53) complex showing that the local motion of the corresponding bases in ACGCC is constrained by the $Asn^{12}$ and $Gln^{45}$ residues, respectively (Figure 5). Though the effect of NC on the fluorescence properties of the 2Ap-labeled ODNs is qualitatively similar to that of glycerol, it differs by an important aspect. Indeed, glycerol induces similar increases of the 2Ap quantum yield in the four ODNs due to a mechanical decrease of the number of collisions of 2Ap with its neighbors by viscosity. In contrast, NC differently affects the dynamics of the bases at positions 2 and 5, since the quantum yield of 2Ap in AApCGCC increases by only 2.5-fold while it increases by about 7-fold in AACGApC. Moreover, NC does not affect the local motion rate of 2Ap at position 2 while it slows down the local motion of the probe at position 5. This slowing down may be due to an interaction of 2Ap at position 5 with the side chain of $Gln^{45}$ (Figure 5) since a H-bond was reported between this

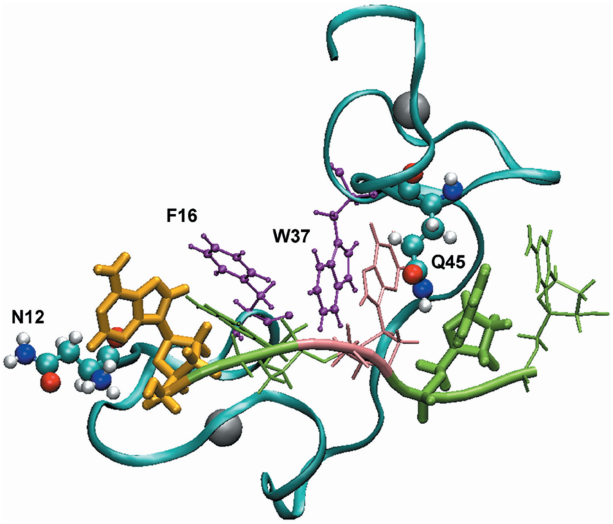


**Figure 5.** Structure of the NC(12-53)/ACGCC complex. NC protein backbone, blue ribbon; $Phe^{16}$ and $Trp^{37}$ residues, magenta. Zinc atoms are as gray spheres. The side chains of $Asn^{12}$ and $Gln^{45}$ are represented in CPK color code. The A (yellow) and C (green) residues of the ODN which have been substituted by 2Ap in our study are in bold. The G residue that interacts with $Trp^{37}$ is in pink.

$Gln^{45}$ side chain and the corresponding C residue in the ACGCC/NC(12-53) complex (11). Alternatively, the effect on the local motion of 2Ap may also be an indirect consequence of the interaction of its neighbors with NC. In this respect, the strong fluorescence increase of 2Ap at position 5 (giving a fluorescence quantum yield that is only five times lower than that of the free ODN) is likely a consequence of the strong stacking of G4 with the $Trp^{37}$ residue that freezes the mobility of G4 and thus restricts its collisions with 2Ap (11,29). Moreover, this stacking also rotates the guanine residue in respect to the phosphate ribose axis, further preventing its collisions with 2Ap. In contrast, the stacking of C3 with $Phe^{16}$ appears less stable and constrained since two orientations of this couple were found in the complex. Moreover, the A1 residue likely protrudes out of the complex and is thus quite mobile. Thus, both C3 and A1 residues are still able to collide with 2Ap in this complex, explaining its efficient quenching.

The fluorescence signal of 2Ap can also be used to characterize the complex of AATGCC with NC. From the strong similarities of the steady state and time-resolved fluorescence parameters of AACGApC and AATGApC complexed with NC, it can be inferred that G4 stacks similarly with the $Trp^{37}$ residue in both complexes. More generally, since the 3′ half of the ODNs interacts mainly with the distal finger of NC, this interaction is likely similar in both complexes. In contrast, the stronger NC-induced increase of 2Ap fluorescence in AApTGCC as compared to AApCGCC suggests that the flexibility of the 5′ half of the ODN is more strongly decreased by NC in the former sequence. This observation may be related to a stronger interaction of T3 as compared to C3 with NC, due to a stable interaction of the methyl group of T3 with the aromatic protons of $Phe^{16}$ as well as with the methyl

groups of $Val^{13}$ as $Thr^{24}$ (N. Morellet, personal communication). This stable interaction with T3 may strongly hinder its collisions with 2Ap. Alternatively, the binding of T3 to NC may favor a direct interaction of NC with 2Ap, preventing its collisions with neighbor bases. However, the absence of change in the rate of the 2Ap local motion does not favor this hypothesis. The more 'frozen' complex obtained with the TG-containing sequence is in line with its stronger binding constant as compared to the CG-containing sequence (29).

Comparison of the native NC with the truncated NC(11-55) derivative indicated that the finger domain plays a central role in restricting the ODN flexibility and local dynamics of 2Ap at positions 2 and 5. In AApTGCC, both the ODN flexibility and 2Ap local dynamics are further restricted by the terminal basic domain of NC (Table 1). The stronger dependence of the fluorescence parameters of AApTGCC as compared to AApCGCC on the N-terminal domain suggests that this domain interacts tighter with 2Ap at position 2 in the former ODN. This tight interaction is likely a consequence of a different binding mode of the proximal NC finger to AApTGCC that orientates differently the N-terminal domain.

In sharp contrast to NC(11-55), $(SSHS)_2$NC(11-55) minimally affects the fluorescence parameters of the four tested 2Ap-labeled ODNs. This does not result from a decreased binding level since this mutant was shown to bind to various ODNs with high affinity (40,46). The poor effect of $(SSHS)_2$NC(11-55) is likely a consequence of its inability to restrict the ODN flexibility and 2Ap local dynamics. As a result, the distribution of the 2Ap conformers and the quenching of 2Ap by its neighbors are similar to those in the free ODN. Thus, the folding of the finger domain appears critical for restricting the ODN flexibility and 2Ap local dynamics. This crucial role of folding is likely related to the hydrophobic platform (formed by the $Val^{13}$, $Phe^{16}$, $Thr^{24}$, $Ala^{25}$, $Trp^{37}$ and $Met^{46}$ residues) at the folded finger surface that plays a key role in ODN binding (10,11,40,53) and specific structural changes (10–12). In line with this hypothesis, only a limited stacking of $Trp^{37}$ with the ODN bases was observed in the complexes with $(SSHS)_2$NC(11-55), as shown by the limited decrease of $Trp^{37}$ fluorescence (data not shown). This explains that the G4 residue is not 'frozen' by stacking with $Trp^{37}$ and can thus efficiently quench 2Ap at the position 5 in the complex. Stacking interactions with $Phe^{16}$ may be prevented as well in the complexes with $(SSHS)_2$NC(11-55) since the interaction of $Phe^{16}$ with ACGCC has been shown to be largely altered with a NC mutant exhibiting a distorted proximal finger (11). The limited restriction of the mobility of the ODN bases in the complexes with $(SSHS)_2$NC(11-55) is in line with a binding of the unfolded peptide mainly to the phosphate backbone. This binding is likely mediated mainly through electrostatic interactions that compensate for the loss of hydrophobic interactions with the bases (40,46). Since unfolded NC peptides are unable to destabilize the secondary structure of cTAR (40) and alter the cooperativity of the helix–coil transition of λ DNA molecules (54), the restriction of the ODN flexibility and local dynamics of the bases is certainly essential for the destabilizing component of NC chaperone activity. In addition, since mutations that prevent the folding of the finger domain lead to completely noninfectious viruses (6–9), 'freezing' of the ODN dynamics may be a key feature of NC during the viral life cycle.

The relationship between the restriction of the ODN dynamics and the biological activities of NC was further substantiated with the $A^{16}$NC(11-55) and $L^{37}$NC(11-55) mutants. Both mutations led to fully noninfectious viruses (6), likely by altering the nucleic acid binding and chaperone properties of NC (40,42,46,48). With $A^{16}$NC(11-55), the local dynamics of 2Ap at position 5 and its close neighbors was restricted to the same level than with NC(11-55) while in contrast, the local dynamics of 2Ap at position 2 in the presence of $A^{16}$NC(11-55) was comparable to that in the free ODNs. Accordingly, the distal finger of $A^{16}$NC(11-55) likely interacts with the 3′ half of the ODN sequences in the same way than the unmodified NC(11-55). In contrast, the $Phe^{16}\rightarrow$Ala mutation deeply modified the interaction of the proximal finger with the 5′ half of the ODN sequences, probably due to the inability of $Ala^{16}$ to interact with C3 and prevent its rapid collisions with 2Ap at position 2. Symmetric effects were observed with the $L^{37}$NC(11-55) mutant, which showed a strongly reduced ability to prevent quenching of 2Ap at position 5. This indicates that $Leu^{37}$ is probably unable to interact with the G4 base and thus cannot prevent the fast collisions of this residue with 2Ap at position 5. In addition, the change induced by $L^{37}$NC(11-55) in the rate of the 2Ap local motion further suggests that in contrast to the unmodified peptide, the $Gln^{45}$ residue of $L^{37}$NC(11-55) does probably not interact with 2Ap at position 5 in the complex. Nevertheless, in contrast to $(SSHS)_2$NC(11-55), both $A^{16}$NC(11-55) and $L^{37}$NC(11-55) mutants restrict the overall ODN flexibility, as shown by the absence of any contribution from segmental motions in the long rotational correlation time of their complexes with the 2Ap-labeled ODNs (Table 2). Accordingly, the complexes with these two mutants are probably stabilized through hydrophobic interactions between the correctly folded fingers of the mutants and the ODN bases. Taken together, the data with the $A^{16}$NC(11-55) and $L^{37}$NC(11-55) mutants unambiguously confirmed that the aromatic residues of the hydrophobic plateau at the top of the folded fingers play a key role in the nucleic acid recognition and the restriction of the ps–ns local dynamics of the nucleotide subdomains to which they bind.

In conclusion, 2Ap fluorescence allowed us to characterize sub-nanosecond and nanosecond dynamics of NC target hexanucleotides and their complexes with NC. The effects of NC binding on 2Ap fluorescence are explained by restriction of the ODN flexibility and 2Ap local mobility that impedes collisions of 2Ap with neighbor bases and thus, largely decreases its dynamic quenching. This is consistent with the 'adaptive binding' model of protein–nucleic acid interaction where the conformational freedom of single-stranded ODNs becomes restricted due to protein binding. The 'freezing' of the ODN flexibility seemed to be mainly supported by the folded

zinc finger domain. The restriction of the local dynamics of the bases was more specifically attributed to the hydrophobic platform at the top of the folded fingers and notably, to the stacking of $Trp^{37}$ with the G base and the interaction of $Phe^{16}$ with the preceding C base. Since this hydrophobic plateau also supports the NC chaperone properties and notably the ability of NC to destabilize the stem of various stem-loops (40), the restriction of the ps–ns ODN dynamics is likely a mechanistic component of these properties. In this respect, together with the increase in the distance and the rotation of the consecutive bases which interact with $Phe^{16}$ and $Trp^{37}$ (10,11), the restriction of the local motion of these bases and their close neighbors may induce the disruption of base pairs in the double strand segments destabilized by NC (32,55–59). Thus, the NC-induced distortion of the ODN structure and local 'freezing' of the bases likely constitute the initial events responsible notably for the NC-chaperoned opening/closing of the cTAR DNA stem (56,60–62). Moreover, the NC-induced conformational changes and restriction of the local base motion probably favor the interaction of the loops of stem-loop sequences with their complementary sequences, explaining the loop–loop promoted annealing of (–)PBS/(+)PBS (63) and mini-TAR sequences (64) as well as the NC-promoted formation of PBS (65,66) and DIS (67) kissing loop homodimers. These hypotheses on the dependence of NC chaperone properties on the NC-promoted changes in the local dynamics of various 2Ap-labeled stem-loop sequences are currently investigated. Finally, since the NC-induced changes in the 2Ap fluorescence parameters were shown to depend on the position and the context of the probe, 2Ap can be used to site-specifically report on the binding of NC to more complex sequences.

## ACKNOWLEDGEMENTS

We acknowledge N. Morellet for providing the NMR data on the AATGCC/NC complex and fruitful discussion. This work was funded by Agence Nationale de Recherches sur le SIDA (peptide synthesizer); the European Commission Consortium 'Targeting Replication and Integration of HIV'; Fondation pour la Recherche Medicale, France (ACE2005120624 to S.V.A.). Funding to pay the Open Access publication charges for this article was provided by Agence Nationale de Recherches sur le SIDA.

*Conflict of interest statement*. None declared.

## REFERENCES

1. Darlix,J.L., Cristofari,G., Rau,M., Pechoux,C., Berthoux,L. and Roques,B. (2000) Nucleocapsid protein of human immunodeficiency virus as a model protein with chaperoning functions and as a target for antiviral drugs. *Adv. Pharmacol.*, **48**, 345–372.
2. Clever,J., Sassetti,C. and Parslow,T.G. (1995) RNA secondary structure and binding sites for gag gene products in the 5′ packaging signal of human immunodeficiency virus type 1. *J. Virol.*, **69**, 2101–2109.
3. De Rocquigny,H., Gabus,C., Vincent,A., Fournie-Zaluski,M.C., Roques,B. and Darlix,J.L. (1992) Viral RNA annealing activities of human immunodeficiency virus type 1 nucleocapsid protein require only peptide domains outside the zinc fingers. *Proc. Natl Acad. Sci. USA*, **89**, 6472–6476.
4. Bampi,C., Jacquenet,S., Lener,D., Decimo,D. and Darlix,J.L. (2004) The chaperoning and assistance roles of the HIV-1 nucleocapsid protein in proviral DNA synthesis and maintenance. *Int. J. Biochem. Cell Biol.*, **36**, 1668–1686.
5. D'Souza,V. and Summers,M.F. (2005) How retroviruses select their genomes. *Nat. Rev. Microbiol.*, **3**, 643–655.
6. Dorfman,T., Luban,J., Goff,S.P., Haseltine,W.A. and Gottlinger,H.G. (1993) Mapping of functionally important residues of a cysteine-histidine box in the human immunodeficiency virus type 1 nucleocapsid protein. *J. Virol.*, **67**, 6159–6169.
7. Gorelick,R.J., Gagliardi,T.D., Bosche,W.J., Wiltrout,T.A., Coren,L.V., Chabot,D.J., Lifson,J.D., Henderson,L.E. and Arthur,L.O. (1999) Strict conservation of the retroviral nucleocapsid protein zinc finger is strongly influenced by its role in viral infection processes: characterization of HIV-1 particles containing mutant nucleocapsid zinc-coordinating sequences. *Virology*, **256**, 92–104.
8. Guo,J., Wu,T., Anderson,J., Kane,B.F., Johnson,D.G., Gorelick,R.J., Henderson,L.E. and Levin,J.G. (2000) Zinc finger structures in the human immunodeficiency virus type 1 nucleocapsid protein facilitate efficient minus- and plus-strand transfer. *J. Virol.*, **74**, 8980–8988.
9. Ottmann,M., Gabus,C. and Darlix,J.L. (1995) The central globular domain of the nucleocapsid protein of human immunodeficiency virus type 1 is critical for virion structure and infectivity. *J. Virol.*, **69**, 1778–1784.
10. De Guzman,R.N., Wu,Z.R., Stalling,C.C., Pappalardo,L., Borer,P.N. and Summers,M.F. (1998) Structure of the HIV-1 nucleocapsid protein bound to the SL3 psi-RNA recognition element. *Science*, **279**, 384–388.
11. Morellet,N., Demene,H., Teilleux,V., Huynh-Dinh,T., de Rocquigny,H., Fournie-Zaluski,M.C. and Roques,B.P. (1998) Structure of the complex between the HIV-1 nucleocapsid protein NCp7 and the single-stranded pentanucleotide d(ACGCC). *J. Mol. Biol.*, **283**, 419–434.
12. Amarasinghe,G.K., De Guzman,R.N., Turner,R.B. and Summers,M.F. (2000) NMR structure of stem-loop SL2 of the HIV-1 psi RNA packaging signal reveals a novel A-U-A base-triple platform. *J. Mol. Biol.*, **299**, 145–156.
13. Walker,J.R., Corpina,R.A. and Goldberg,J. (2001) Structure of the Ku heterodimer bound to DNA and its implications for double-strand break repair. *Nature*, **412**, 607–614.
14. Mazin,A.V., Zaitseva,E., Sung,P. and Kowalczykowski,S.C. (2000) Tailed duplex DNA is the preferred substrate for Rad51 protein-mediated homologous pairing. *EMBO J.*, **19**, 1148–1156.
15. Zhang,Q., Sun,X., Watt,E.D. and Al-Hashimi,H.M. (2006) Resolving the motional modes that code for RNA adaptation. *Science*, **311**, 653–656.
16. Mollova,E.T. (2002) Single-molecule fluorescence of nucleic acids. *Curr. Opin. Chem. Biol.*, **6**, 823–828.
17. Ward,D.C., Reich,E. and Stryer,L. (1969) Fluorescence studies of nucleotides and polynucleotides. I. Formycin, 2-aminopurine riboside, 2,6-diaminopurine riboside, and their derivatives. *J. Biol. Chem.*, **244**, 1228–1237.
18. Jean,J.M. and Hall,K.B. (2001) 2-Aminopurine fluorescence quenching and lifetimes: role of base stacking. *Proc. Natl Acad. Sci. USA*, **98**, 37–41.
19. Jean,J.M. and Hall,K.B. (2004) Stacking-unstacking dynamics of oligodeoxynucleotide trimers. *Biochemistry*, **43**, 10277–10284.
20. O'Neill,M.A. and Barton,J.K. (2002) 2-Aminopurine: a probe of structural dynamics and charge transfer in DNA and DNA:RNA hybrids. *J. Am. Chem. Soc.*, **124**, 13053–13066.
21. Fiebig,T., Wan,C. and Zewail,A.H. (2002) Femtosecond charge transfer dynamics of a modified DNA base: 2-aminopurine in complexes with nucleotides. *Chem. Phys. Chem.*, **3**, 781–788.
22. Wan,C., Fiebig,T., Schiemann,O., Barton,J.K. and Zewail,A.H. (2000) Femtosecond direct observation of charge transfer between bases in DNA. *Proc. Natl Acad. Sci. USA*, **97**, 14052–14055.
23. Bradrick,T.D. and Marino,J.P. (2004) Ligand-induced changes in 2-aminopurine fluorescence as a probe for small molecule binding to HIV-1 TAR RNA. *RNA*, **10**, 1459–1468.

24. Somsen,O.J., Keukens,L.B., de Keijzer,M.N., van Hoek,A. and van Amerongen,H. (2005) Structural heterogeneity in DNA: temperature dependence of 2-aminopurine fluorescence in dinucleotides. *Chem. Phys. Chem.*, **6**, 1622–1627.
25. Rachofsky,E.L., Osman,R. and Ross,J.B. (2001) Probing structure and dynamics of DNA with 2-aminopurine: effects of local environment on fluorescence. *Biochemistry*, **40**, 946–956.
26. Kaul,M., Barbieri,C.M. and Pilch,D.S. (2004) Fluorescence-based approach for detecting and characterizing antibiotic-induced conformational changes in ribosomal RNA: comparing aminoglycoside binding to prokaryotic and eukaryotic ribosomal RNA sequences. *J. Am. Chem. Soc.*, **126**, 3447–3453.
27. Hariharan,C. and Reha-Krantz,L.J. (2005) Using 2-aminopurine fluorescence to detect bacteriophage T4 DNA polymerase-DNA complexes that are important for primer extension and proofreading reactions. *Biochemistry*, **44**, 15674–15684.
28. Ramreddy,T., Rao,B.J. and Krishnamoorthy,G. (2007) Site-specific dynamics of strands in ss- and dsDNA as revealed by time-domain fluorescence of 2-aminopurine. *J. Phys. Chem. B*, **111**, 5757–5766.
29. Vuilleumier,C., Bombarda,E., Morellet,N., Gerard,D., Roques,B.P. and Mely,Y. (1999) Nucleic acid sequence discrimination by the HIV-1 nucleocapsid protein NCp7: a fluorescence study. *Biochemistry*, **38**, 16816–16825.
30. Fisher,R.J., Rein,A., Fivash,M., Urbaneja,M.A., Casas-Finet,J.R., Medaglia,M. and Henderson,L.E. (1998) Sequence-specific binding of human immunodeficiency virus type 1 nucleocapsid protein to short oligonucleotides. *J. Virol.*, **72**, 1902–1909.
31. de Rocquigny,H., Ficheux,D., Gabus,C., Fournie-Zaluski,M.C., Darlix,J.L. and Roques,B.P. (1991) First large scale chemical synthesis of the 72 amino acid HIV-1 nucleocapsid protein NCp7 in an active form. *Biochem. Biophys. Res. Commun.*, **180**, 1010–1018.
32. Bernacchi,S., Stoylov,S., Piemont,E., Ficheux,D., Roques,B.P., Darlix,J.L. and Mely,Y. (2002) HIV-1 nucleocapsid protein activates transient melting of least stable parts of the secondary structure of TAR and its complementary sequence. *J. Mol. Biol.*, **317**, 385–399.
33. Lakowicz,J.R. (1999) *Principles of Fluorescence Spectroscopy*, 2nd edn. Kluwer Academic/Plenum Publishers, New York, p.304.
34. Lipari,G. and Szabo,A. (1980) Effect of librational motion on fluorescence depolarization and nuclear magnetic resonance relaxation in macromolecules and membranes. *Biophys. J.*, **30**, 489–506.
35. Rai,P., Cole,T.D., Thompson,E., Millar,D.P. and Linn,S. (2003) Steady-state and time-resolved fluorescence studies indicate an unusual conformation of 2-aminopurine within ATAT and TATA duplex DNA sequences. *Nucleic Acids Res.*, **31**, 2323–2332.
36. Nag,N., Ramreddy,T., Kombrabail,M., Krishna Mohan,P.M., D'Souza,J., Rao,B.J., Duportail,G., Mely,Y. and Krishnamoorthy,G. (2006) Dynamics of DNA and protein-DNA complexes viewed through time-domain fluorescence. In Geddes,C. and Lakowicz,J.R. (eds), *Reviews in Fluorescence*, Springer Science, New York, Vol. 3, pp. 311–340.
37. Guest,C.R., Hochstrasser,R.A., Sowers,L.C. and Millar,D.P. (1991) Dynamics of mismatched base pairs in DNA. *Biochemistry*, **30**, 3271–3279.
38. Xu,D., Evans,K.O. and Nordlund,T.M. (1994) Melting and premelting transitions of an oligomer measured by DNA base fluorescence and absorption. *Biochemistry*, **33**, 9592–9599.
39. Larsen,O.F., van Stokkum,I.H., Gobets,B., van Grondelle,R. and van Amerongen,H. (2001) Probing the structure and dynamics of a DNA hairpin by ultrafast quenching and fluorescence depolarization. *Biophys. J.*, **81**, 1115–1126.
40. Beltz,H., Clauss,C., Piemont,E., Ficheux,D., Gorelick,R.J., Roques,B., Gabus,C., Darlix,J.L., de Rocquigny,H. *et al.* (2005) Structural determinants of HIV-1 nucleocapsid protein for cTAR DNA binding and destabilization, and correlation with inhibition of self-primed DNA synthesis. *J. Mol. Biol.*, **348**, 1113–1126.
41. Mely,Y., De Rocquigny,H., Morellet,N., Roques,B.P. and Gerad,D. (1996) Zinc binding to the HIV-1 nucleocapsid protein: a thermodynamic investigation by fluorescence spectroscopy. *Biochemistry*, **35**, 5175–5182.
42. Fisher,R.J., Fivash,M.J., Stephen,A.G., Hagan,N.A., Shenoy,S.R., Medaglia,M.V., Smith,L.R., Worthy,K.M., Simpson,J.T. *et al.* (2006) Complex interactions of HIV-1 nucleocapsid protein with oligonucleotides. *Nucleic Acids Res.*, **34**, 472–484.
43. Cruceanu,M., Gorelick,R.J., Musier-Forsyth,K., Rouzina,I. and Williams,M.C. (2006) Rapid kinetics of protein-nucleic acid interaction is a major component of HIV-1 nucleocapsid protein's nucleic acid chaperone function. *J. Mol. Biol.*, **363**, 867–877.
44. Maki,A.H., Ozarowski,A., Misra,A., Urbaneja,M.A. and Casas-Finet,J.R. (2001) Phosphorescence and optically detected magnetic resonance of HIV-1 nucleocapsid protein complexes with stem-loop sequences of the genomic Psi-recognition element. *Biochemistry*, **40**, 1403–1412.
45. Amarasinghe,G.K., Zhou,J., Miskimon,M., Chancellor,K.J., McDonald,J.A., Matthews,A.G., Miller,R.R., Rouse,M.D. and Summers,M.F. (2001) Stem-loop SL4 of the HIV-1 psi RNA packaging signal exhibits weak affinity for the nucleocapsid protein. structural studies and implications for genome recognition. *J. Mol. Biol.*, **314**, 961–970.
46. Urbaneja,M.A., Kane,B.P., Johnson,D.G., Gorelick,R.J., Henderson,L.E. and Casas-Finet,J.R. (1999) Binding properties of the human immunodeficiency virus type 1 nucleocapsid protein p7 to a model RNA: elucidation of the structural determinants for function. *J. Mol. Biol.*, **287**, 59–75.
47. Bombarda,E., Ababou,A., Vuilleumier,C., Gerard,D., Roques,B.P., Piemont,E. and Mely,Y. (1999) Time-resolved fluorescence investigation of the human immunodeficiency virus type 1 nucleocapsid protein: influence of the binding of nucleic acids. *Biophys. J.*, **76**, 1561–1570.
48. Remy,E., de Rocquigny,H., Petitjean,P., Muriaux,D., Theilleux,V., Paoletti,J. and Roques,B.P. (1998) The annealing of tRNA3Lys to human immunodeficiency virus type 1 primer binding site is critically dependent on the NCp7 zinc fingers structure. *J. Biol. Chem.*, **273**, 4819–4822.
49. Jean,J.M. and Hall,K.B. (2002) 2-Aminopurine electronic structure and fluorescence properties in DNA. *Biochemistry*, **41**, 13152–13161.
50. Krishnamoorthy,G., Roques,B., Darlix,J.L. and Mely,Y. (2003) DNA condensation by the nucleocapsid protein of HIV-1: a mechanism ensuring DNA protection. *Nucleic Acids Res.*, **31**, 5425–5432.
51. Ramos,A., Gubser,C.C. and Varani,G. (1997) Recent solution structures of RNA and its complexes with drugs, peptides and proteins. *Curr. Opin. Struct. Biol.*, **7**, 317–323.
52. Leulliot,N. and Varani,G. (2001) Current topics in RNA-protein recognition: control of specificity and biological function through induced fit and conformational capture. *Biochemistry*, **40**, 7947–7956.
53. Stote,R.H., Kellenberger,E., Muller,H., Bombarda,E., Roques,B.P., Kieffer,B. and Mely,Y. (2004) Structure of the His44 –> Ala single point mutant of the distal finger motif of HIV-1 nucleocapsid protein: a combined NMR, molecular dynamics simulation, and fluorescence study. *Biochemistry*, **43**, 7687–7697.
54. Williams,M.C., Rouzina,I., Wenner,J.R., Gorelick,R.J., Musier-Forsyth,K. and Bloomfield,V.A. (2001) Mechanism for nucleic acid chaperone activity of HIV-1 nucleocapsid protein revealed by single molecule stretching. *Proc. Natl Acad. Sci. USA*, **98**, 6121–6126.
55. Beltz,H., Azoulay,J., Bernacchi,S., Clamme,J.P., Ficheux,D., Roques,B., Darlix,J.L. and Mely,Y. (2003) Impact of the terminal bulges of HIV-1 cTAR DNA on its stability and the destabilizing activity of the nucleocapsid protein NCp7. *J. Mol. Biol.*, **328**, 95–108.
56. Azoulay,J., Clamme,J.P., Darlix,J.L., Roques,B.P. and Mely,Y. (2003) Destabilization of the HIV-1 complementary sequence of TAR by the nucleocapsid protein through activation of conformational fluctuations. *J. Mol. Biol.*, **326**, 691–700.
57. Liu,H.W., Cosa,G., Landes,C.F., Zeng,Y., Kovaleski,B.J., Mullen,D.G., Barany,G., Musier-Forsyth,K. and Barbara,P.F. (2005) Single-molecule FRET studies of important intermediates in the nucleocapsid-protein-chaperoned minus-strand transfer step in HIV-1 reverse transcription. *Biophys. J.*, **89**, 3470–3479.
58. Liu,H.W., Zeng,Y., Landes,C.F., Kim,Y.J., Zhu,Y., Ma,X., Vo,M.N., Musier-Forsyth,K. and Barbara,P.F. (2007) Insights on the role of nucleic acid/protein interactions in chaperoned nucleic acid rearrangements of HIV-1 reverse transcription. *Proc. Natl Acad. Sci. USA*, **104**, 5261–5267.

59. Hong,M.K., Harbron,E.J., O'Connor,D.B., Guo,J., Barbara,P.F., Levin,J.G. and Musier-Forsyth,K. (2003) Nucleic acid conformational changes essential for HIV-1 nucleocapsid protein-mediated inhibition of self-priming in minus-strand transfer. *J. Mol. Biol.*, **325**, 1–10.
60. Beltz,H., Piemont,E., Schaub,E., Ficheux,D., Roques,B., Darlix,J.L. and Mely,Y. (2004) Role of the structure of the top half of HIV-1 cTAR DNA on the nucleic acid destabilizing activity of the nucleocapsid protein NCp7. *J. Mol. Biol.*, **338**, 711–723.
61. Cosa,G., Harbron,E.J., Zeng,Y., Liu,H.W., O'Connor,D.B., Eta-Hosokawa,C., Musier-Forsyth,K. and Barbara,P.F. (2004) Secondary structure and secondary structure dynamics of DNA hairpins complexed with HIV-1 NC protein. *Biophys. J.*, **87**, 2759–2767.
62. Cosa,G., Zeng,Y., Liu,H.W., Landes,C.F., Makarov,D.E., Musier-Forsyth,K. and Barbara,P.F. (2006) Evidence for non-two-state kinetics in the nucleocapsid protein chaperoned opening of DNA hairpins. *J. Phys. Chem. B*, **110**, 2419–2426.
63. Ramalanjaona,N., Rocquigny,H.D., Millet,A., Ficheux,D., Darlix,J.L. and Mely,Y. (2007) Investigating the mechanism of the nucleocapsid protein chaperoning of the second strand transfer during HIV-1 DNA synthesis. *J. Mol. Biol.*, **374**, 1074–1053.
64. Vo,M.N., Barany,G., Rouzina,I. and Musier-Forsyth,K. (2006) Mechanistic studies of mini-TAR RNA/DNA annealing in the absence and presence of HIV-1 nucleocapsid protein. *J. Mol. Biol.*, **363**, 244–261.
65. Egele,C., Schaub,E., Ramalanjaona,N., Piemont,E., Ficheux,D., Roques,B., Darlix,J.L. and Mely,Y. (2004) HIV-1 nucleocapsid protein binds to the viral DNA initiation sequences and chaperones their kissing interactions. *J. Mol. Biol.*, **342**, 453–466.
66. Egele,C., Schaub,E., Piemont,E., de Rocquigny,H. and Mely,Y. (2005) Investigation by fluorescence correlation spectroscopy of the chaperoning interactions of HIV-1 nucleocapsid protein with the viral DNA initiation sequences. *C. R. Biol.*, **328**, 1041–1051.
67. Rist,M.J. and Marino,J.P. (2002) Mechanism of nucleocapsid protein catalyzed structural isomerization of the dimerization initiation site of HIV-1. *Biochemistry*, **41**, 14762–14770.